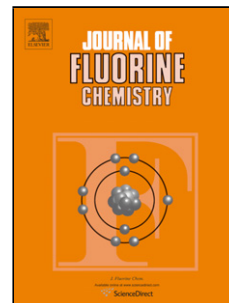


Accepted Manuscript

Title: Liquid crystal and photo-induced properties of polymers carrying pyridylazobenzene groups and iodopentafluorobenzene rings self-assembled through halogen bond



Authors: Cinthya Valeska Castro-Pérez, Nayely Trejo-Carbajal, Rosa Julia Rodríguez-González, Leticia Larios-López, Isaura Felix-Serrano, Dámaso Navarro-Rodríguez

PII: S0022-1139(19)30060-0
DOI: <https://doi.org/10.1016/j.jfluchem.2019.05.003>
Reference: FLUOR 9325

To appear in: *FLUOR*

Received date: 14 February 2019
Revised date: 3 May 2019
Accepted date: 3 May 2019

Please cite this article as: Castro-Pérez CV, Trejo-Carbajal N, Rodríguez-González RJ, Larios-López L, Felix-Serrano I, Navarro-Rodríguez D, Liquid crystal and photo-induced properties of polymers carrying pyridylazobenzene groups and iodopentafluorobenzene rings self-assembled through halogen bond, *Journal of Fluorine Chemistry* (2019), <https://doi.org/10.1016/j.jfluchem.2019.05.003>

This is a PDF file of an unedited manuscript that has been accepted for publication. As a service to our customers we are providing this early version of the manuscript. The manuscript will undergo copyediting, typesetting, and review of the resulting proof before it is published in its final form. Please note that during the production process errors may be discovered which could affect the content, and all legal disclaimers that apply to the journal pertain.

Liquid crystal and photo-induced properties of polymers carrying pyridylazobenzene groups and iodopentafluorobenzene rings self-assembled through halogen bond

Cinthya Valeska Castro-Pérez, Nayely Trejo-Carbajal, Rosa Julia Rodríguez-González,
Leticia Larios-López, Isaura Felix-Serrano, Dámaso Navarro-Rodríguez*

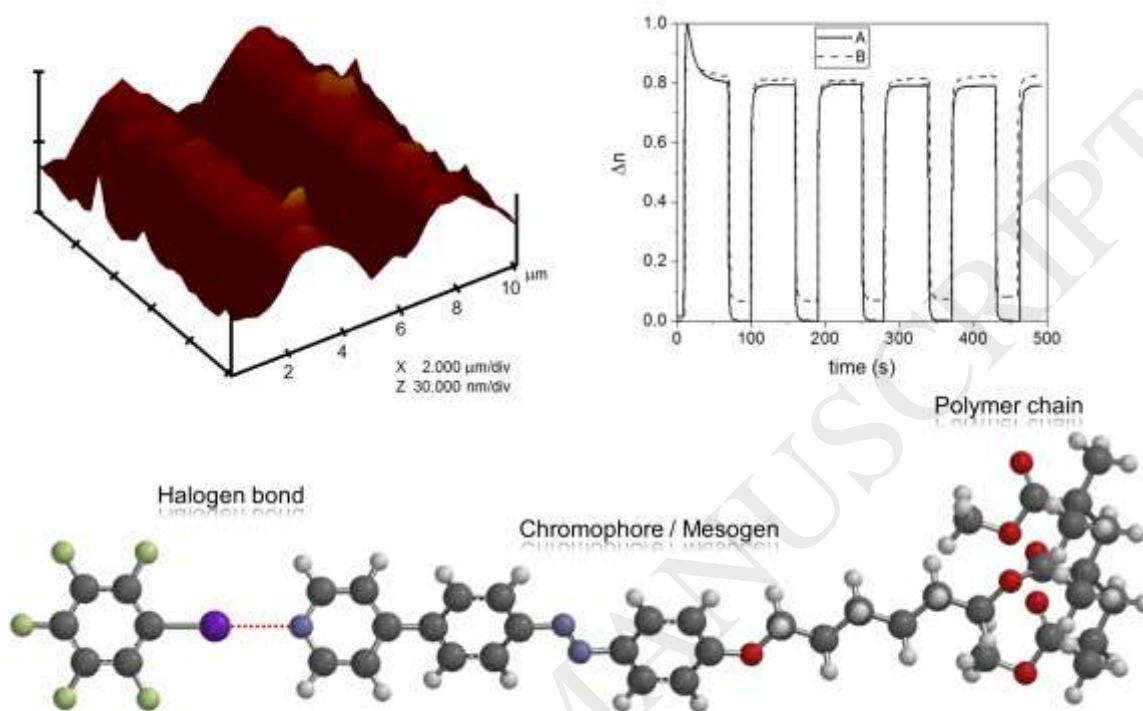
Departamento de Materiales Avanzados, Centro de Investigación en Química Aplicada
(CIQA), Boulevard Enrique Reyna H. 140, 25254, Saltillo Coahuila, Mexico

Corresponding author: Dámaso Navarro-Rodríguez

Phone: 52 (844)4389846; Fax: 52 (844)4389839

e.mail: damaso.navarro@ciqa.edu.mx

Graphical abstract



Highlights

- Polymers carrying pyridylazobenzenes and iodopentafluorobenzene rings self-assembled through halogen bond were synthesized.
- The halogen-bonded complexes showed liquid crystals properties of the smectic type.
- The halogen-bonded complexes showed good photo-induced isomerization despite the bulkiness of the chromophore units.
- Halogen-bonded complexes showed a quite good photo-response in both writing/erasure experiments and SRGs inscription.

Abstract

In this work, we report on the synthesis, liquid crystal behavior and photo-induced optical properties of a polymer and a copolymer, both carrying lateral pyridylazobenzene groups and iodopentafluorobenzene (IPFB) rings self-assembled through halogen bond. The formation of the halogen-bonded complexes was confirmed by Fourier transform infrared (FTIR) spectroscopy; the mesomorphic behavior was determined by differential scanning calorimetry (DSC), polarizing optical microscopy (POM) and X-ray diffraction (XRD); and the optical properties were photo-induced with a 405 nm laser beam. The pyridylazobenzene-functionalized polymer showed a smectic-type order (smectic A and crystE phases) whereas the copolymer and the halogen-bonded complexes with IPFB rings formed aggregates whose molecular order in the z-coordinates is suppressed (no layers). The photo-isomerization (in solution) of the polymer and copolymer led to a *trans*-to-*cis* isomer conversion (%*cis*) of 82, and 95, respectively. In film, the %*cis* values resulted much inferior but still high enough to induce optical properties, as for instance, in films of the copolymer (%*cis* = 60) and its halogen-bonded complex (%*cis* = 46) that responded quite well in periodical light-induced writing/erasure experiments. Only the halogen-bonded copolymer complex allowed us to register regular surface relief gratings (SRGs) suggesting that it would be a good candidate for optical data storage applications.

Keyword: Azopolymer; Halogen bond; Self-assembly; Liquid crystal; Fluorine

INTRODUCTION

Azobenzenes are organic chromophores that have been widely and deeply studied over the last two decades for their unique photo-induced optical properties and broad

potential application in different fields [1-4]. It turns out that azobenzenes move at molecular, nanometric, and micrometric levels while they photo-isomerize upon irradiation with linearly polarized light [5]. At molecular level, these chromophores absorb light and generate successive *trans-cis-trans* isomerization cycles that move and reorient themselves until reaching a photo-stationary state. At nanometric level (domain level), the coordinated photo-induced reorientation of chromophores induces molecular alignment that is reflected in anisotropic properties such as birefringence and dichroism [6]. Finally, at micrometer scale, a mass transport causes regular surface deformations, which are best known as surface relief gratings (SRGs) [7]. The nano- and micro-scale motions work fairly well for azopolymers; i.e. for polymer chains carrying azobenzene groups [5]. Much less frequent are the low-molar mass azocompounds exhibiting both high degree of photo-alignment and efficient formation of regular SRGs [8]. In azopolymers, azobenzene groups can be either attached to polymer chains through covalent links [9] or assembled with the polymer chains through weak electrostatic forces like the hydrogen and halogen bonds [10-12]. A new or different class of azopolymer is that in which its covalently-linked azobenzene groups interact with small molecules through hydrogen bond (ex. polymethacrylate carrying lateral azopyridine groups interacting with benzoic acid molecules), resulting in materials with modified thermal and optical properties [13]. The hydrogen bond is attracting because it allows the preparation of complexes through self-assembly, which is an important area of current science [14-16]. Their parent complexes linked through halogen bond are still poorly known. The halogen bond has characteristics that parallel those of the hydrogen bond in terms of strength, and can be either stronger or weaker, although, differently to the hydrogen bond, it is hydrophobic and highly directional [17,18]. Up to date, few halogen-bonded assemblies carrying azobenzene groups have been reported, and some of them have

revealed to be very good photo-responsive materials for the induction of SRGs, which, by the way, showed one of the highest modulation depths (up to 2.4 times the film thickness) reported so far for azocompounds [19]. The high directionality of the halogen bond interaction seems promote an efficient mass transport, as deduced by Saccone et al. in comparing similar hydrogen and halogen-bonded polymer-azobenzene supramolecular complexes of similar chemical structure [20]. The azobenzene-based halogen-bonded complexes have also shown a fairly good photomechanical energy transfer to photo-passive polymers, suggesting that they are good candidates for applications in solid state functional elements [21].

The azopolymer can be amorphous, crystalline or liquid crystal; the latter is highly attracting because it combines the peculiar balance of order and fluidity of liquid crystals [22] with both, the capability of azobenzenes to be reoriented (or aligned) under light stimuli [23] and the ability of polymers to form films [9]. The combination of these three characteristics in one single material can result in improved photo-induced properties. It is noteworthy to mention that, the photo-induced orientation of azobenzenes and the spontaneous self-organization of liquid crystals (when the azobenzene derivative is a mesogen) create synergy or cooperative molecular motions, leading to high birefringence, which is a property of practical interest [6,24]. Here in, we report on the synthesis as well as on the liquid crystal and photo-induced optical properties of a polymer and a copolymer carrying pyridylazobenzene groups and iodopentafluorobenzene (IPFB) rings self-assembled through halogen bond.

2. EXPERIMENTAL PART

2.1 Materials

4-bromophenol, 1,6-dibromohexane, hydrochloric acid, 4-hydroxyaniline, iodopentafluorobenzene (IPFB), methacrylic acid, methyl methacrylate (MMA), 4-pyridinylboronic acid, sodium carbonate, sodium hydroxide, sodium nitrite, azobisisobutyronitrile (AIBN), and tetrakis(triphenylphosphine)palladium (0) (or Pd[0]). All these reagents were purchased from Sigma-Aldrich and used without further purification unless otherwise noted. Reactive grade acetone, chloroform (CHCl₃), dimethylformamide (DMF), ethyl acetate and hexanes were purchased from Fermont and used without further purification. Tetrahydrofuran (THF) was dried over sodium / benzophenone and distilled right before use. AIBN was recrystallized twice from methanol and MMA was purified by vacuum distillation.

2.2. Synthesis

The route for the synthesis of the pyridylazobenzene-functionalized polymer, copolymer, and their corresponding halogen-bonded complexes is outlined in Scheme 1. For simplicity reasons, the intermediates and final polymers were all labeled with sequential numbers. Initially, the azobenzene precursor **1** was synthesized from 4-hydroxyaniline and 4-bromophenol following the azocoupling method described elsewhere [25]. Then, the end bromo-functionalized azobenzene **2** was obtained from **1** and 1,6-dibromohexane through a Williamson reaction [26]. Next, the pyridylazobenzene derivative **3** was obtained via a Suzuki-Miyaura cross-coupling reaction between **2** and 4-pyridinylboronic acid using Pd[0] as catalyst [22]. In a further step, **3** was reacted with methacrylic acid to obtain a pyridylazobenzene-functionalized methacrylic monomer **4**,

which was next polymerized by free radicals (AIBN, THF, 65 °C, 72 h), into its corresponding polymer **5** as well as into a copolymer with MMA (labeled as copolymer **6**). Monomer **4** and MMA are randomly distributed along the polymer chain. Finally, **5** and **6** were mixed with IPFB in solution (chloroform as solvent) to obtain the halogen-bonded complexes namely polymer-IPFB complex **7** and copolymer-IPFB complex **8**, respectively.

2.3 Instruments

The structure of intermediates and final polymers was confirmed by proton (^1H NMR) and carbon (^{13}C NMR) nuclear magnetic resonance spectroscopies, using a Bruker 400 MHz spectrometer (CDCl_3 as solvent), and by Fourier transform infrared (FTIR) spectroscopy (ATR method), using an iS50 Nicolet spectrophotometer. The thermal stability of polymers was determined with a thermogravimetric analyzer (TGA) from TA Instruments Q500, connected to a N_2 vector gas, and heating at 10 °C min^{-1} from 30 to 800 °C. TGA traces were included in supporting information (SI). The thermal behavior was determined with a differential scanning calorimeter (DSC) from TA Instruments Q2000 at heating and cooling rates of 10 °C/min from -20 to 200 °C ; reported DSC traces correspond to the first cooling and second heating scans. The average molecular weights of polymers were measured by size exclusion chromatography (SEC), in an Agilent PL-GPC 50, equipped with refractive index detector. THF was used as solvent and polystyrene standards as reference. The optical textures of the liquid crystal phases were registered at different temperatures on cooling from the isotropic liquid, using a polarizing optical microscope (POM) from Olympus, which was coupled to a FP82HT heating plate from Mettler. The X-ray diffraction (XRD) analysis was performed with a small- and wide-angle

X-ray scattering (SWAXS) system from Anton Paar (SAXSessmc²) equipped with a sample holder unit (TCS 300-C), an image plate detector, and temperature control unit (TCU50). X-rays (Cu k_{α} radiation, $\lambda = 0.154$ nm) were generated at 50 mA. The UV-vis spectra were recorded in a Cary 5000 UV-vis-NIR spectrophotometer (Varian), using a standard quartz cell and spectrophotometric grade THF (solution concentrations of ~ 0.04 mg mL⁻¹). The *trans*-to-*cis* isomerization of the monomer, polymer and copolymer was photo-induced (in solution) with unpolarized UV light from a 365 nm UVGL-58 lab-lamp. The copolymer **6** and its complex **8** were also irradiated in film. Films were prepared by spin-coating (solutions of 25 mg mL⁻¹ and rates of 500, 1000 and 1500 rpm) in a rotating processor WS-650 from Laurell Technologies Corporation.

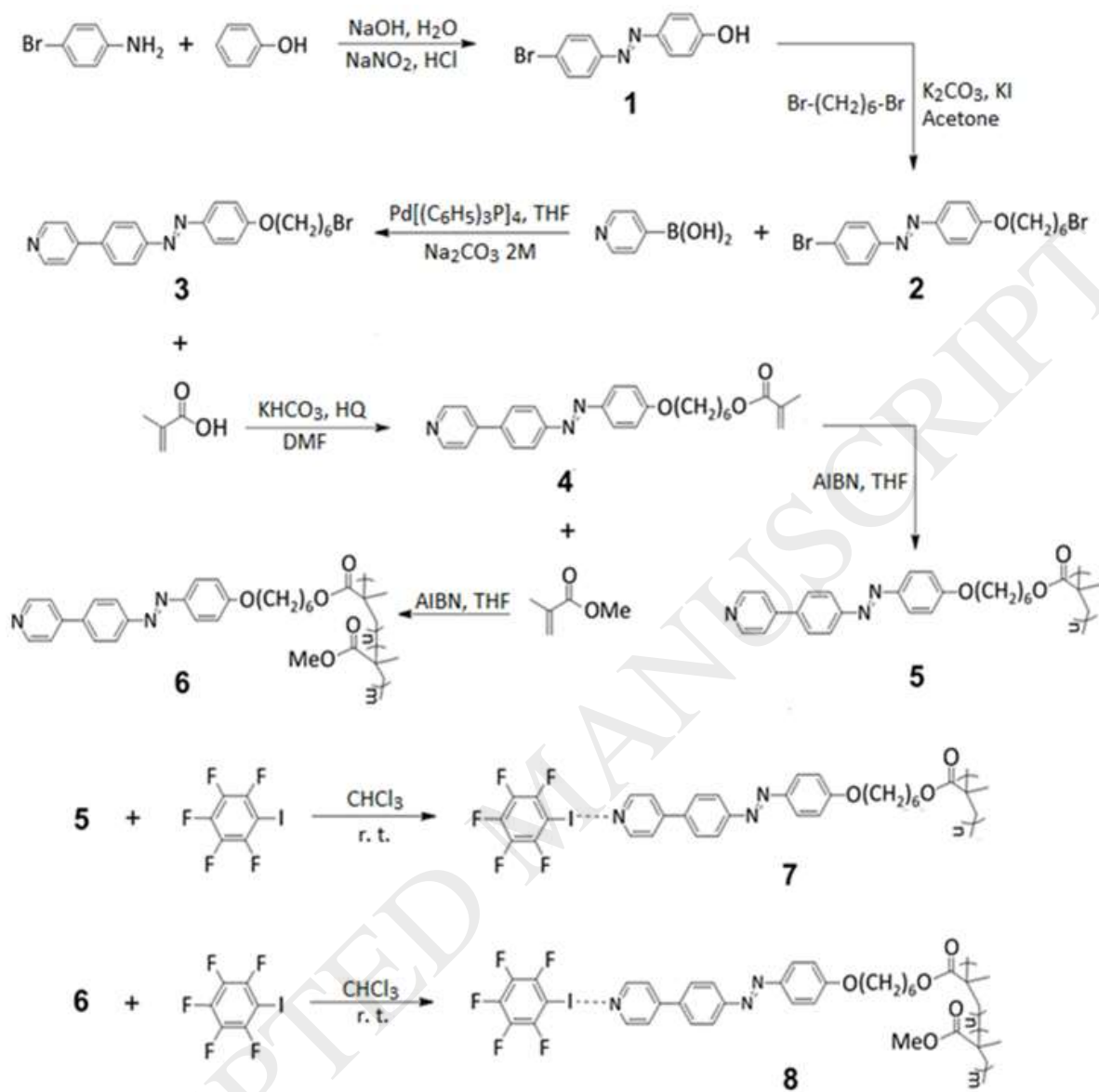
Light-induced birefringence (Δn) experiments were performed with spin coated films, which were irradiated with a linearly polarized laser beam ($\lambda = 405$ nm, 30 mW) while a second laser beam ($\lambda = 633$ nm 12 mW, with an incidence angle of 45°) was used as a probe. The change in the polarization state was measured with a Stokes polarimeter [9]. The SRGs were inscribed (or photo-induced) in casted films of the copolymer **6** and its complex **8**, employing the Lloyd arrangement. A 405 nm laser beam was split into two equal intensity beams (right and left circularly polarized) that hit the sample in the same spot with an incident angle of 4° during 15 min. The shape and modulation depth of the inscribed SRGs were determined by atomic force microscopy (AFM-3100 from DIVEeco).

3. RESULTS AND DISCUSSION

3.1. Synthesis and chemical characterization

Experimental procedures for the synthesis of the intermediates **1** and **2** were described in a previous report [27]. The pyridylazobenzene derivative (intermediate **3**) was synthesized from **2** and 4-pyridinylboronic acid via the Suzuki-Miyaura cross-coupling reaction using Pd[0] as catalyst. This intermediate was obtained as a yellow solid (poorly soluble powder) at 57% yield. The ^1H NMR spectrum of **3** (Figure 1A) shows two doublets at 8.69 (q and q') and 7.56 ppm (p and p'), confirming the right coupling of the pyridine fragment to the azobenzene core. The other proton signals of **3** match well with those of the azocompound **2** whose ^1H NMR spectrum was reported in a previous work [27]. The reaction of **3** with methacrylic acid gave the monomer **4** as a yellow solid at 94% yield. The ^1H NMR spectrum of **4** shows one singlet at 1.97 ppm that was assigned to the methyl protons (t) of the methacrylic fragment, and two multiplets at 5.57 and 6.12 ppm attributed to the two protons (u) of the vinyl group (Figure 1B). It can be also noted that **4** no-longer shows the triplet at 3.5 ppm, corresponding to the protons (a) of the methylene group located in α position to the bromine atom in its precursor **3**, and to which the methacrylic acid has been chemically attached. The polymerization of **4**, via free radicals (AIBN/THF), gave the polymer **5** (77% yield; M_w : 2230 g mol $^{-1}$) whose ^1H NMR spectrum is also depicted in Figure 1 (spectrum C). As expected, the two multiplets at 5.57 and 6.12 ppm, attributed to the protons of the vinyl group, no-longer appear in the spectrum, and all signals became broader as it is characteristic of polymeric molecules. **5** was also characterized by FTIR spectroscopy (cm $^{-1}$): 2939 (ν_a , CH $_2$), 2864 (ν_s , CH $_2$), 1722 (ν , C=O), 1595 (ν , -C=N- pyridine), 1543, 1499, 1471 (ν , C=C), 1394 (δ_s , C-H CH $_3$ group), 1248 (ν_a , C $_{ar}$ -O-C), 1139 (ν_a , O-C-C), 991 (δ , pyridine-phenyl), and 814 (δ , C $_{ar}$ -H).

The polymer-IPFB complex (**7**) was prepared by introducing equimolar amounts of **5** (0.135 mmol) and IPFB (0.135 mmol) into chloroform (2 mL) at room temperature. The solution was held under stirring for 30 min before allow the chloroform to evaporate at room temperature. The obtained orange powder (fine crystals) was characterized by FTIR spectroscopy (cm^{-1}): 2938 (ν_{a} , CH_2), 2863 (ν_{s} , CH_2), 1722 (ν , $\text{C}=\text{O}$), 1596 (ν $-\text{C}=\text{N}-$ pyridine), 1543, 1413 (ν , $\text{C}=\text{C}$), 1508, 1484 (ν , $\text{C}=\text{C}$, fluorinated aromatic ring), 1394 (δ_{s} , CH_3), 1248 (ν_{a} , $\text{C}_{\text{ar}}-\text{O}-\text{C}$), 1138 (ν_{a} , $\text{O}-\text{C}-\text{C}$), 1079 (ν , $\text{C}-\text{I}$ + ring def.), 1000 cm^{-1} (CF -str.), 998 (δ , pyridine-phenyl), 971 (ν_{s} , $\text{C}-\text{F}$), 814 (δ_{ar} , ring def.), and 803 cm^{-1} (ν $\text{C}-\text{I}$ + ring def.). The position (wavenumber) of some of these bands was compared before and after complexation. Such comparison is shown in Figure 2 where the FTIR spectrum of **7** (Figure 2B) is depicted along with those of its precursors **5** (Figure 2A) and IPFB (Figure 2C) in an expanded wavenumber range from 600 to 1200 cm^{-1} . Their full FTIR spectrum (500 to 3300 cm^{-1}) can be found in *supplemental information* (S2). As expected, the FTIR spectrum of **7** is a combination of the FTIR spectra of **5** and IFBP, although, in this peculiar mixture, some small changes (highlighted with dotted lines and small arrows in Figure 2B), either in the position (wavenumber) or in the band intensity, were appreciated. Such small changes were associated to the halogen bond interaction as it is explained in the next paragraph.



Scheme 1. General route for the synthesis of the polymer-IPFB (**7**) and copolymer-IPFB (**8**) halogen-bonded complexes.

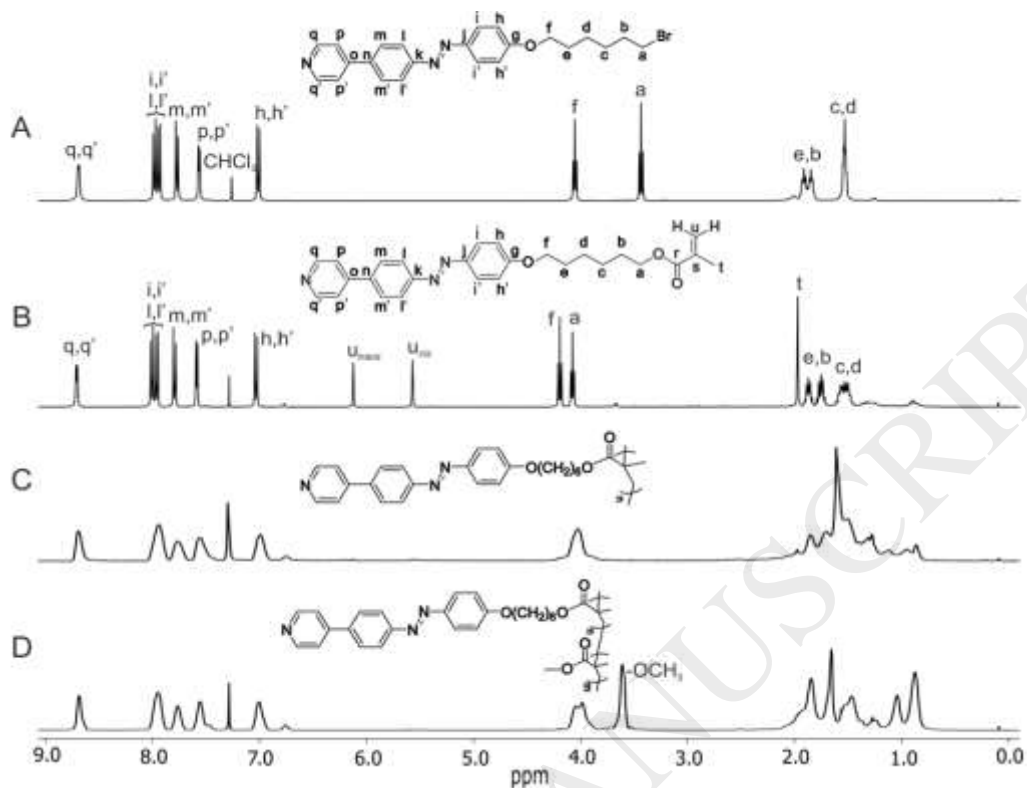


Figure 1. ¹H NMR spectra of the intermediate **3** (A), the monomer **4** (B), the polymer **5** (C), and the copolymer **6** (D). Solvent CDCl₃.

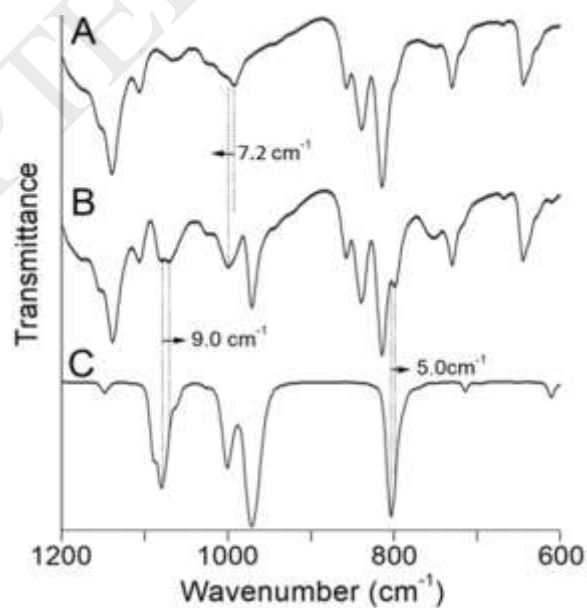


Figure 2. FTIR spectra of the polymer **5** (A), polymer-IPFB complex **7** (B), and IPFB (C).

Table 1. Vibrational modes for IPFB and polymer-IPFB complex, lying in the 750 and 1100 cm^{-1} frequency range of the FTIR spectrum.

Vibration mode	IPFB ν (cm^{-1})	Polymer-IPFB complex ν (cm^{-1})
C–I str. + ring def.	803	798
C–F str.	971	971
C–F str.	1000	1000
ring def. + C–I str.	1079	1070

It was reported that the FTIR spectroscopy lets detect the occurrence of the halogen bond interaction between pyridine and iodoperfluorocarbons [28]. Such an interaction produces a red-shift in the C–F stretching bands (appearing in the 800 to 1200 cm^{-1} spectral region) that is normally attributed to the increase of the electron density of the perfluorinated moiety (electron acceptor) upon complexation. It can also produce blue-shifts of some fundamental bands of the pyridine ring. The lack of hydrogen atoms in the IPFB ring leads to most fundamental bands lying in a narrow range below 1700 cm^{-1} [29]. In the FTIR spectrum of the IPFB (Figure 2C) such fundamental bands appeared at 803 (C–I str. + ring def.), 971 (C–F str.), 1000 (CF-str.), and 1079 cm^{-1} (ring def. + C–I str.). As expected, the all four bands appeared in the FTIR spectrum of the polymer-IPFB complex **7**, but they are weak and overlapped with some other bands (Figure 2B). A close inspection let us see that the bands at 971 and 1000 cm^{-1} remained at the same wavenumber as compared with the corresponding ones of the pure IPFB, however, the bands situated at 803 and 1079 cm^{-1} in the spectrum of the IPFB ring appeared at 798 and 1070 cm^{-1} in that of the complex; i.e. red-shifted by 5 and 9 cm^{-1} , respectively (Table 1). Such red shifts are

associated to the halogen bond interaction occurring between the nitrogen atom of the pyridine ring and the iodine atom of IPFB, as it is represented (model molecule) for a monomeric unit in Figure 3. Red-shifts of similar order were already reported for some FTIR bands of the perfluorinated part of the pyridine–perfluoroalkyliodide [30], pyrene–1,4-diiodotetrafluorobenzene [31], and alkoxystilbazole–perfluoroalkyldiiodide [28] halogen-bonded complexes, when they are compared with those of their corresponding pure perfluoro compound. On the other hand, the vibrational modes of the pyridine rings remained almost unaltered under the halogen bond complexation with IPFB; the only difference in the spectrum of the polymer-IPFB complex **7**, with respect to that of the non-complexed polymer **5**, is the blue shifting (7.2 cm^{-1}) of the band around 990 cm^{-1} . The blue-shift is likely to be associated with the higher positive charge (lower electron density) of the pyridine cycle [28]. The difference in micro-environments around the pyridylazobenzene ring, before and after complexation, might also play a role in both vibrational frequency and strength of fundamental bands, but their effect might be relatively weak. The higher intensity of the vibrational mode around 750 cm^{-1} (γ_{ar} , ring oop def. of the whole pyridine aromatic system [32]), may arise from such difference in micro-environments.

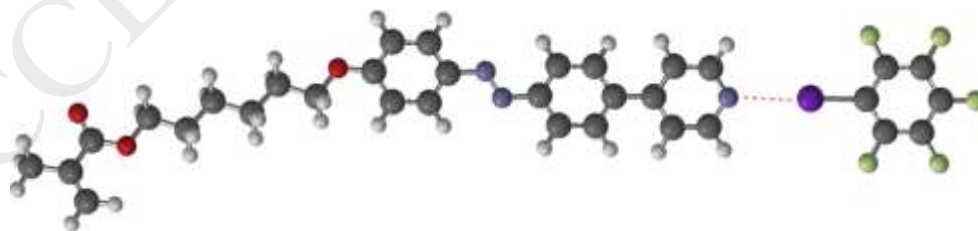


Figure 3. Model molecule of the halogen-bonded complex between a pyridylazobenzene-functionalized methacrylic unit and iodopentafluorobenzene.

The monomer **4** was copolymerized with methyl methacrylate (fed mole ratio of 1:1) via free radicals, using AIBN as initiator and THF as solvent. The random copolymer **6** was obtained at 60% yield and M_w of 4217 g mol^{-1} . The ^1H NMR spectrum of **6** (Figure 1D) is similar to that of **5** (Figure 1C); the main difference is the proton signal at 3.60 ppm, corresponding to the O-CH₃ group of MMA, and from which the actual mole ratio of monomers (1:0.81) was calculated. **6** was also characterized by FTIR (cm^{-1}): 2988 (ν_{as} , C-H), 2945 (ν_{a} , CH₂), 2869 (ν_{s} , CH₂), 1722 (ν , C=O), 1595 (ν , -C=N-), 1544, 1499, 1472 (ν , C=C, ar.), 1393 (δ_{s} , C-H), 1247 (ν_{a} , C_{ar}-O-C), 1138 (ν_{a} , O-C-C), 991 (δ , pyridine-phenyl), and 813 (δ_{ar} , ring def.).

The copolymer-IPFB complex **8** was next obtained from **6** and IPFB following the same methodology described for the preparation of **7**. The FTIR spectrum of **8** (*Supplemental information, S3*) also showed small differences to the superposed FTIR spectra of their precursors **6** and IPFB. Some of the FTIR (cm^{-1}) bands of **8** are: 2994 (ν_{a} , C-H, CH₃ group of the polymeric chain), 2946 (ν_{a} , CH₂), 2869 (ν_{s} , CH₂), 1724 (ν , C=O), 1597 (ν , -C=N- pyridine), 1544 (ν , C=C aromatic ring), 1509, 1485 (ν , C=C, fluorinated ring), 1394 (δ_{s} , C-H for CH₃ group), 1246 (ν_{a} , C_{ar}-O-C), 1139 (ν_{a} , -O-C-C), 1070 (ν , C-I + ring def.), 1000 cm^{-1} (CF-str.), 998 (δ , pyridine-phenyl), 971 (ν_{s} , C-F), 814 (δ_{ar} , ring def.), and 798 cm^{-1} (ν C-I + ring def.). The vibrational modes at 798 and 1070 cm^{-1} appeared also red-shifted as compared to the corresponding ones in the FTIR spectrum of IPFB (803 and 1079 cm^{-1}), also suggesting the complexation of pyridine with IPFB rings through halogen bond.

3.2. Thermotropic behavior

The polymer **5** and the copolymer **6** were first analyzed by TGA to determine their thermal stability. The TGA traces (*supporting information, SI*) showed for **5** and **6** a 2%–decomposition temperature ($T_{2\%}$) of 271 and 218 °C, respectively. In order to avoid degradation, $T_{2\%}$ was taken as the limit temperature for their further thermotropic analysis by DSC, POM and XRD. It is to point out that polymers carrying lateral bulky groups, like the long rigid rod-like pyridylazobenzenes, are difficult to analyze by these techniques because they use to display very broad and low intense thermal transitions and most often they become isotropic at very high temperature. For this reason, the monomer **4** was first studied as a model molecule.

The monomer **4** displayed multiple thermal transitions in both the second heating and the first cooling DSC traces (Figure 4A), suggesting a liquid crystal behavior. At least two mesomorphic regions at temperature intervals of 100–143 °C and 143–166 °C were detected upon heating. Both, the absence in the cooling trace of an exothermic transition around 100 °C, and the presence of exothermic transition in the heating trace, are due to a super cooling process related to a long induction crystallization period [33]. Such behavior was also observed in POM experiments (upon cooling) where this monomer took from 10 to 20 minutes to crystallize once it reached the room temperature. The optical textures shown by **4** were batonets that on cooling turned into a focal conic-fan texture typical of smectic phases (Figure 5). Its XRD patterns (Figure 6) showed, in the low angles region, one sharp diffraction peak (001) related to the stacking period of the smectic layers, and, in the wide angles region, two diffraction peaks superimposed to a broad band. These two peaks match well to an in-plane (or two-dimensional) centered rectangular lattice (110 and

200) [34], whereas the broad band is characteristic of an in-plane random or liquid-like order. The cell parameters ($a = 8.0 \text{ \AA}$ and $b = 5.28 \text{ \AA}$), calculated from the 110 and 200 diffraction peaks, match well to those normally expected for rigid rod-like mesogens packed in a rectangular cell [35]. Neither the POM textures nor the XRD patterns let us detect changes at the transition temperatures already determined from the DSC traces, nevertheless the combined results of these three techniques let us conclude, for the monomer **4**, a smectic A phase at high temperature (between 143 and 166 °C) and a smectic E (or crystal E) phase at low temperature (below 143 °C). The orthogonality of phases was determined from the d_{001}/L ratio, which is slightly higher (1.15) than unity. In this ratio, d_{001} is the experimental layer spacing (31.2 Å) and L is the theoretical length (27.1 Å) of **4** in its most extended conformation, calculated by molecular modelling software (Spartan 10).

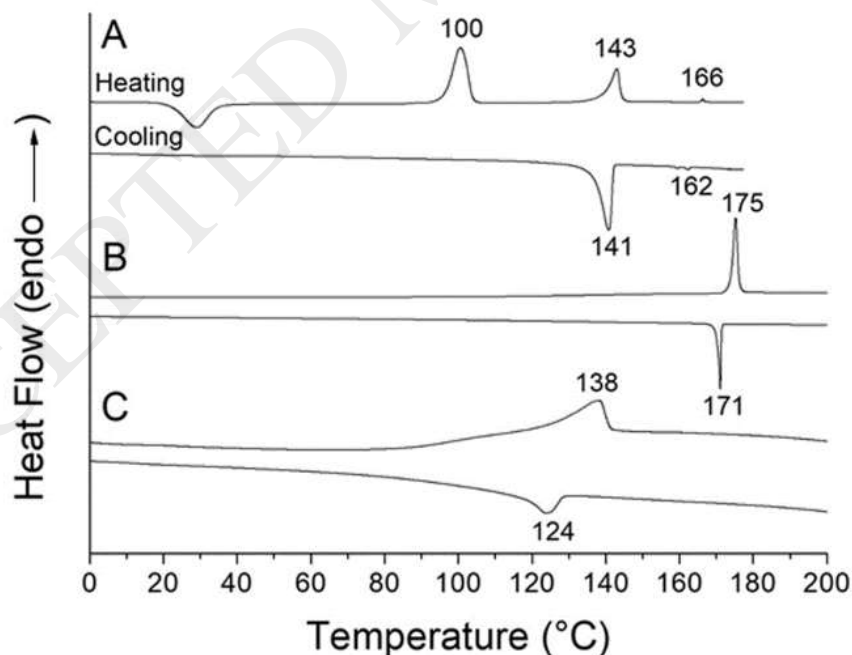


Figure 4. DSC traces of the monomer **4** (A), the polymer **5** (B) and the copolymer **6** (C).

Heating and cooling rates of 10 °C min^{-1} .

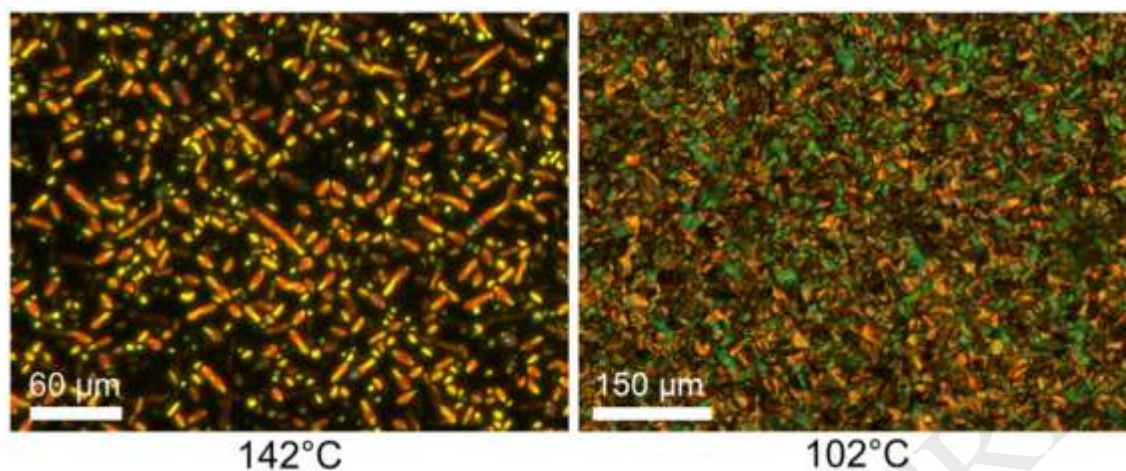


Figure 5. Optical textures of the monomer 4 registered at two different temperatures on cooling from the isotropic phase. Batonets at 142 °C and a focal-conic fan texture at 102 °C.

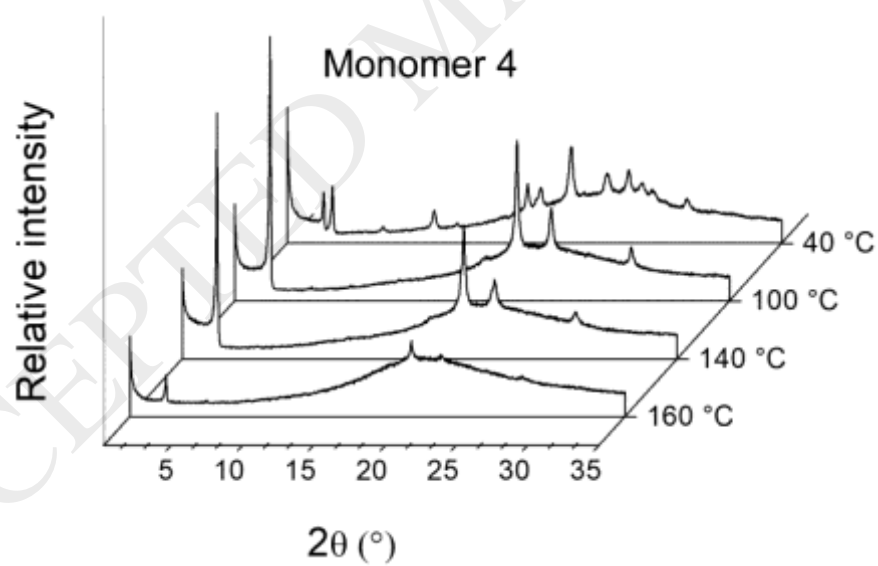


Figure 6. XRD patterns of the monomer 4 registered at four different temperatures on cooling from the isotropic phase.

On the other hand, the polymer **5** displayed one single thermal transition (around 170 °C) in the DSC trace (Figure 4B), suggesting a solid \leftrightarrow liquid transition like that occurring for conventional or non-liquid crystal materials. However, its high-temperature XRD pattern (Figure 7A, 210 °C) showed two equidistant diffraction peaks (001 and 002) at low angles and one broad peak at wide angles. This pattern corresponds to a smectic phase of low order. In cooling to 100 °C, its XRD pattern developed three equidistant diffraction peaks (001, 002, and 003) at low angles and two sharp peaks at wide angles (110 and 200), suggesting a smectic stacking with an in-plane rectangular order. The isotropic phase was not reached in both the DSC and XRD experiments because this polymer starts to decompose below its clearing temperature. The d_{100}/L ratios, calculated from the high (210 °C) and low (100 °C) temperature XRD patterns, were also slightly higher than unity; the smectic phases are therefore of the smectic A and CrytE types. The small diffraction peak around 3.3 Å (28° in 2θ) was attributed to the π -stacking interaction between the pyridylazobenzene cores. A π -stacking distance of 3.3 Å is quite common for the π -stacking of aromatic cores [36]. It must be said that the polymer **5** displayed a thermal transition (see Figure 4B) that is unexpectedly too sharp for a polymeric molecule. The Mw of this polymer, determined by SEC analysis, was only 2230 g mol⁻¹. Such a low molar mass can to certain point explain the sharpness of the transition. We should remark once again that, in the ¹H NMR spectrum of **5** (Figure 1C), all proton signals are broad (typical of polymers) and no vinyl proton signals appeared between 5 and 6.5 ppm.

In a different way to the polymer **5**, the DSC trace of the copolymer **6** showed a broad thermal transition at lower temperature (Figure 4C). Its XRD patterns (Figure 7C) showed two sharp diffraction peaks at wide angles and no peaks in the low angles region. The

existence of two peaks at wide angles suggests an in-plane rectangular order, and the absence of diffraction peaks at low angles means the suppression of molecular order in the z-coordinates (no layers). Molecular arrangements (aggregates) showing only in-plane order were yet reported, as for instance, for rod-like medium-length n-alkanes embedded in a nanoporous structure [37], and for copolymers carrying a reduced number of lateral phenylene-azobenzene chromophores [38]. The complexes **7** and **8** also displayed X-ray patterns (Figures 7B and 7D, respectively) with no peaks at low angles but exhibiting in-plane order, also suggesting the formation of aggregates with no order in the z-coordinates. The presence of aggregates in both polymers (**5** and **6**) and their corresponding complexes (**7** and **8**) was later confirmed by UV-vis experiments as described below.

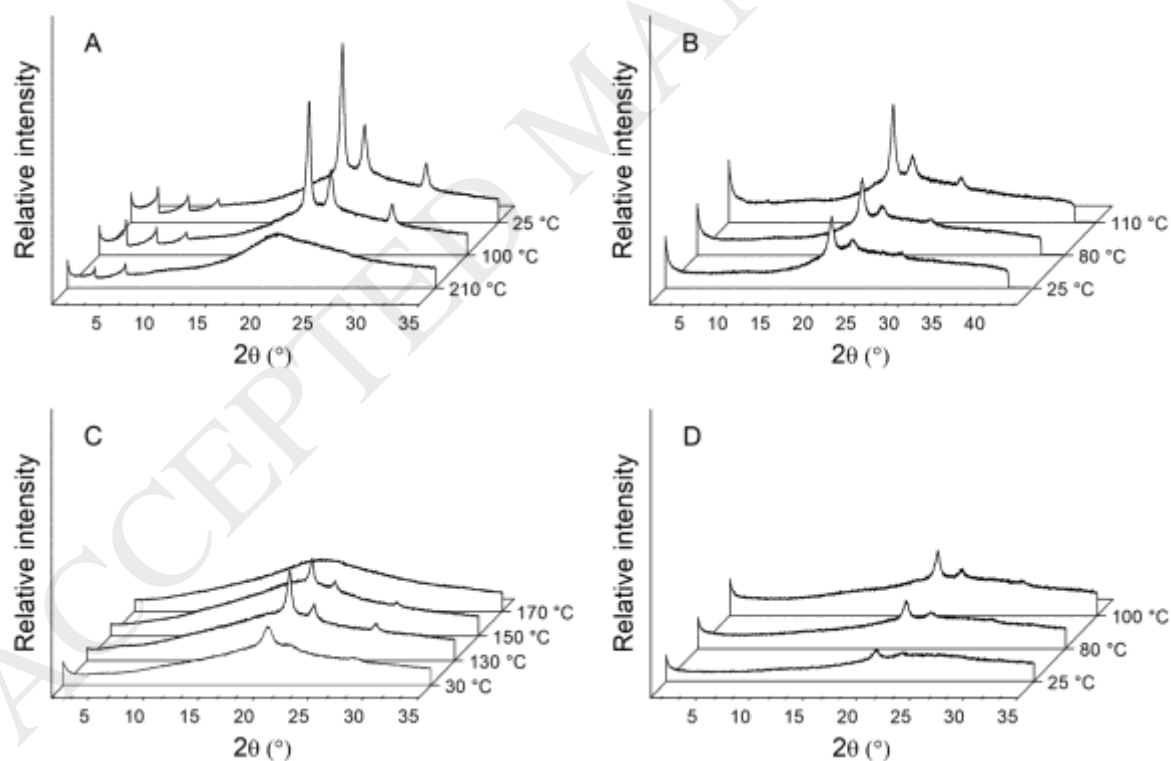


Figure 7. XRD patterns of the polymer **5** (A), polymer-IPFB complex **7** (B), copolymer **6** (C), and copolymer-IPFB complex **8** (D) registered at different temperatures.

3.3 UV-vis spectroscopy

The UV-vis absorption characteristics of chromophores depend on whether they respond as independent units or coupled the ones to the others into excimers, and also into J or H-aggregates [39]. Figure 8A shows the UV-vis absorption spectra of the monomer **4** recorded in solution and film. The spectrum recorded in film is 27 nm - shifted to lower wavelengths as compared to that recorded in solution. Such a relatively high blue (or hypsochromic) shift can be attributed to the formation of H-type aggregates, where chromophores are supposed to be in close proximity to each other and with coplanar transition dipoles [40]. It should be said that the extent of the hypsochromic shift depends on the size of aggregates, as it was demonstrated by our group in a recent work on methacrylic copolymers carrying lateral phenylene(azobenzene) chromophores at variable content (from 5 to 77 mole%) [38]. High blue (or hypsochromic) shifts were attributed to the H-aggregation of the chromophores during smectic phase formation [41]; i.e. extended domains of chromophore units packed in lateral position. This is the case of the monomer **4** that showed a blue-shift of 27 nm and a smectic E-type arrangement at room temperature. The copolymer **6** showed a hypsochromic shift of only 18 nm (Figure 8B), which might correspond to small aggregates. Unfortunately, the polymer **5** was fairly insoluble in a variety of tested solvents and films were not possible to obtain. We faced the same problem in the preparation of the thin and thick films needed for further optical-induced properties.

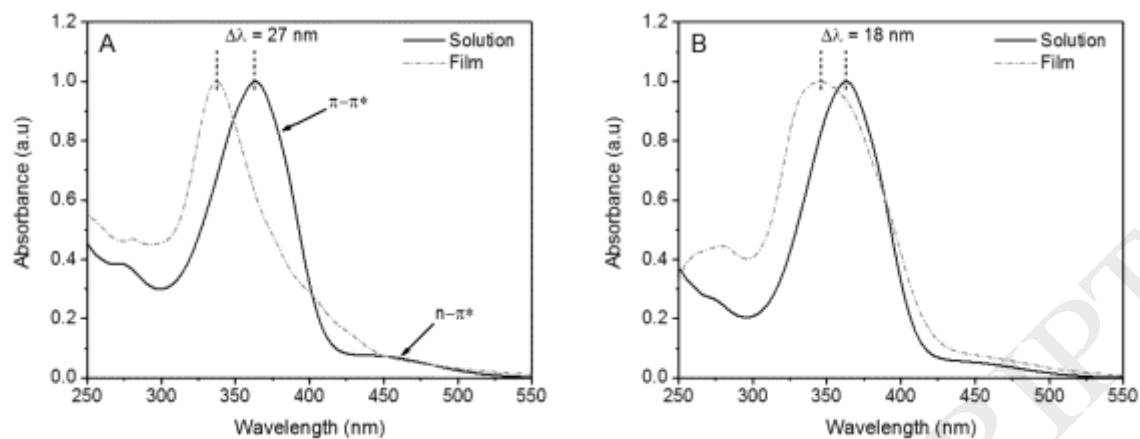


Figure 8. UV-vis absorption spectra of the monomer **4** (A) and copolymer **6** (B) recorded in solution and film. THF was used as solvent.

As mentioned above, one important characteristic of the azo-compounds is their ability to photo-isomerize (*trans* \leftrightarrow *cis*) under UV-vis light stimuli. Such ability is best appreciated in solution, where the chromophores respond as independent units, although, for practical purposes, it is better to determine it in film, where the chromophores can respond in a cooperative way, particularly in pre-ordered semi-crystalline or liquid crystal structures [7]. The monomer **4**, polymer **5** and copolymer **6** were irradiated in solution (THF as solvent) using a 365 nm UV lamp and their resulting spectra were depicted in Figure 9. Before irradiation ($t = 0$ s), all three compounds showed a strong absorption band centered at 363 nm, and a weak band centered at 442 nm. These two bands are due to the $\pi-\pi^*$ and $n-\pi^*$ electronic transitions of the *trans*-isomer, respectively [6]. Once irradiated (at time intervals), the strong absorption band decreased up to reach the photo-stationary state (*PSS*) from which a maximum *cis*-conversion (%*cis*) is determined (Table 2). As expected, **5** attained the lowest %*cis* and the highest *PSS* due to the close approach of chromophores (highly hindered to move) along the chain. We would like to draw your

attention to the fact that the superposed UV-vis spectra of the polymer **5** (Figure 9B) and copolymer **6** (Figure 9C) show isosbestic points only for the first 90 and 120 seconds of irradiation, respectively. After these irradiation times, the isosbestic point at 427 nm is no longer observed, suggesting that a photo-chemical process, other than the *trans*-to-*cis* isomerization, has occurred, although, a further experiment on relaxed solutions (one day on the dark) showed similar absorption spectra as compared to those measured at $t = 0$. This result let us discard the occurrence of side photo-reactions during the irradiation of solutions, as it was already found with azopolymers bearing rigid-rod like azobenzenes [22].

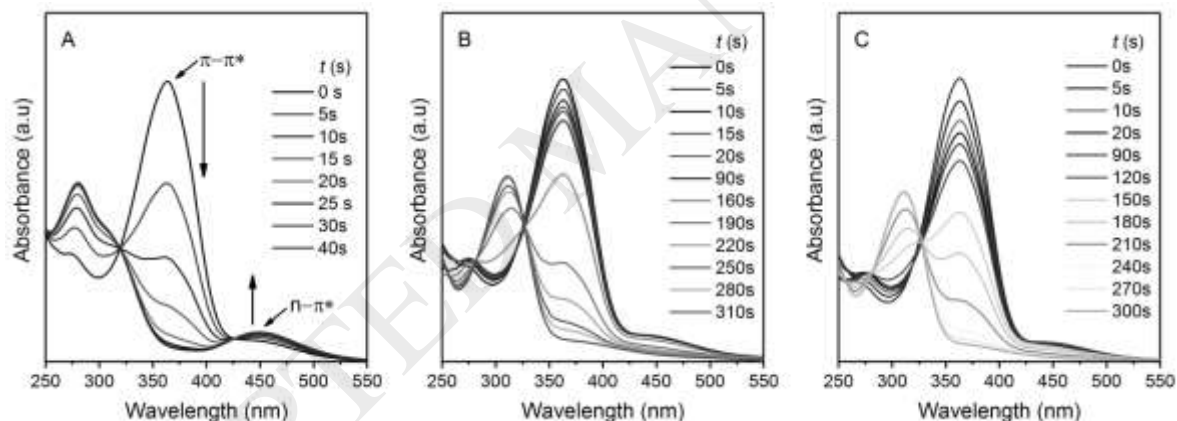


Figure 9. Photo-isomerization kinetics for the monomer **4** (A), polymer **5** (B), and copolymer **6** (C) in solution (THF) irradiated with a 365 nm UV-lamp.

Table 2. Photo-stationary state (*PSS*) and *trans*-to-*cis* photo-conversion at the *PSS* for the monomer **4**, polymer **5**, and copolymer **6**.

Compound	<i>PSS</i> (s)	% <i>cis</i>
4	60	95
5	310	82
6	300	95

Spin-coated films were then prepared for both the copolymer **6** and its complex **8**, which were next irradiated with a UV lamp (363 nm) to induce photo-isomerization at subsequent time intervals (Figure 10). At $t = 0$ s, the light absorption characteristics of **8** are similar to those of **6**, except for a small blue shift. At $t > 0$ s, both the copolymer **6** and its complex **8** showed a rather limited photo-response (%*cis* of 60 and 46, respectively). The relatively low %*cis* reached by the complex implies that the chromophore units are highly restricted to move and photo-isomerize as it occurs for long biphenylene-substituted azobenzenes [42]. It should be reminded that the pyridylazobenzene chromophore becomes longer (or bulkier) under complexation with IPFB. It is noteworthy to mention that the superposed spectra of the irradiated films showed neat isosbestic points all along up to saturation.

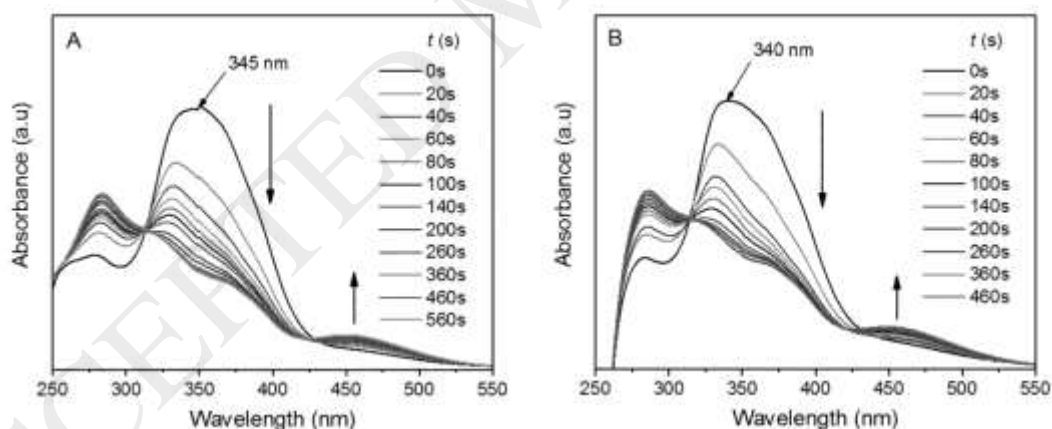


Figure 10. Photo-isomerization kinetics for the copolymer **6** (A) and its complex **8** (B) in film (spin-coated) irradiated with a 365 nm UV-lamp.

3.4 Photo-induced birefringence and surface relief gratings

Solutions of the copolymer **6** and its complex **8** were spin-coated over glass substrates using chloroform solutions (25 mg mL^{-1}). Films (100 to 150 nm thick, respectively) were then irradiated at switch on – switch off cycles with a linearly polarized light (405 nm). The photo-induced birefringence (Δn) versus time plots are depicted in Figure 11. As it can be noted, the photo-alignment is higher for the complex ($\Delta n \sim 0.07$) than for the copolymer ($\Delta n \sim 0.04$), despite the former showed a more restricted photo-isomerization. A similar behavior was found for photo-sensitive azopolymers based on P4VP quaternized with bromo derivative of dialkyloxy-phenyleneazobenzene groups [43]. There in it was proposed that the photo-reorientation depends on the ability of chromophores to move in concert at specific experimental conditions. The complexed chromophores might be tightly held to move in concert upon irradiation.

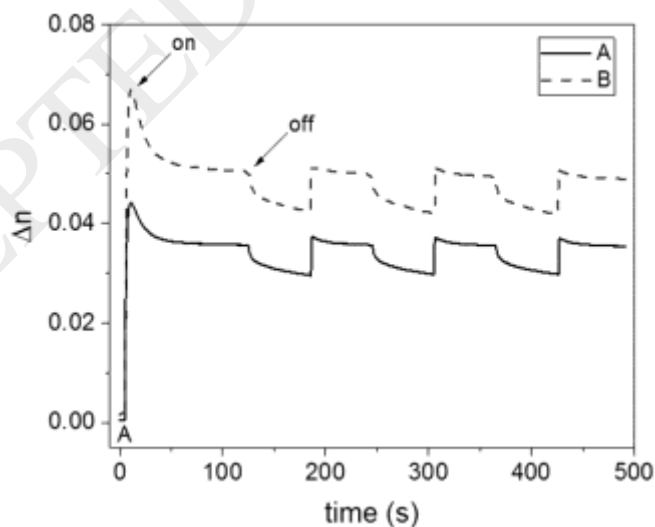


Figure 11. Light-induced birefringence (under switch-on – switch-off cycles) for spin-coated films of the copolymer **6** (A) and its complex **8** (B), both irradiated with a 405 nm linearly polarized laser.

The spin-coated films of the copolymer **6** and its complex **8** were also tested in writing/erasing experiments, using a 405 nm linearly polarized/circularly polarized laser [44]. Plots in Figure 12 shows that both materials respond very fast to the writing and erasing beams, indicating that they are good candidates for optical data storage.

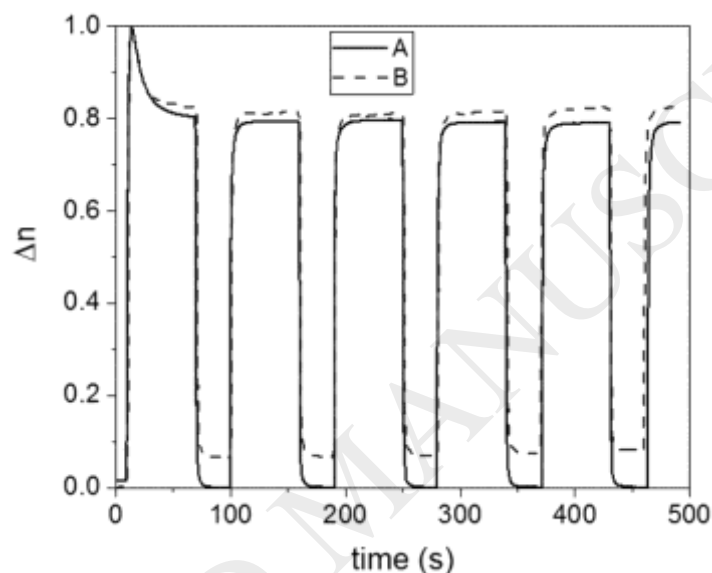


Figure 12. Writing/erasure cycles for the copolymer **6** (A) and its complex **8** (B).

The light-induced mass migration was tested in casted films of the copolymer **6** and its complex **8**. The irradiated films were studied by POM and AFM (Figures 13 and 14), which let us observe small and large irradiated areas (microscale), respectively. POM images are composed of alternated bright and dark lines, which are characteristic of SRGs of regular periodicity [45]. AFM micrographs show a periodic sinusoidal profile with a grating modulation depth of around 50 nm. The AFM micrographs also show clear evidence of agglomerates, particularly for the copolymer **6**, whose SRG is fairly irregular. It is to point out that the SRGs inscription was made in mature films (prepared several days

before irradiation) where agglomerates are yet consolidated and therefore the chromophore units move under constrains. The irradiation of fresh films (irradiated few hours after preparation) may result in SRGs with a more regular profile as demonstrated in a previous work on polymers carrying chromophore units of similar length [43].

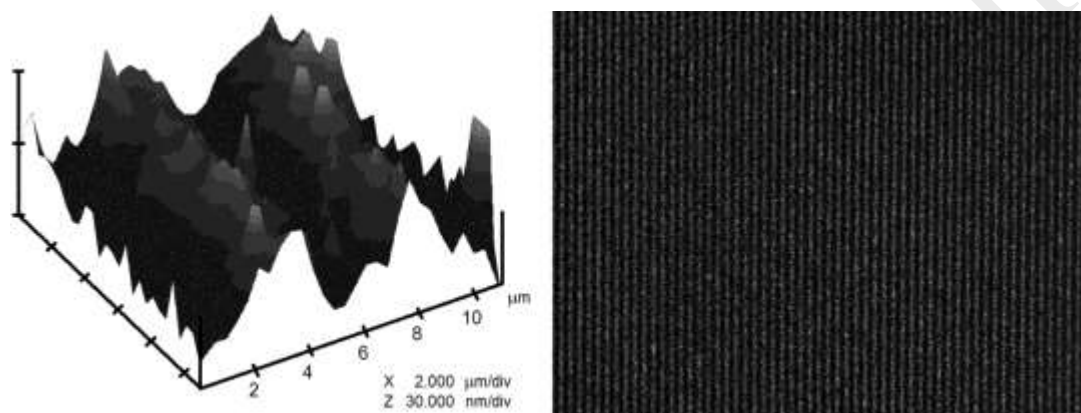


Figure 13. AFM (*left*) and POM (*right*) images of a SRG photo-inscribed in a film of the copolymer **6**.

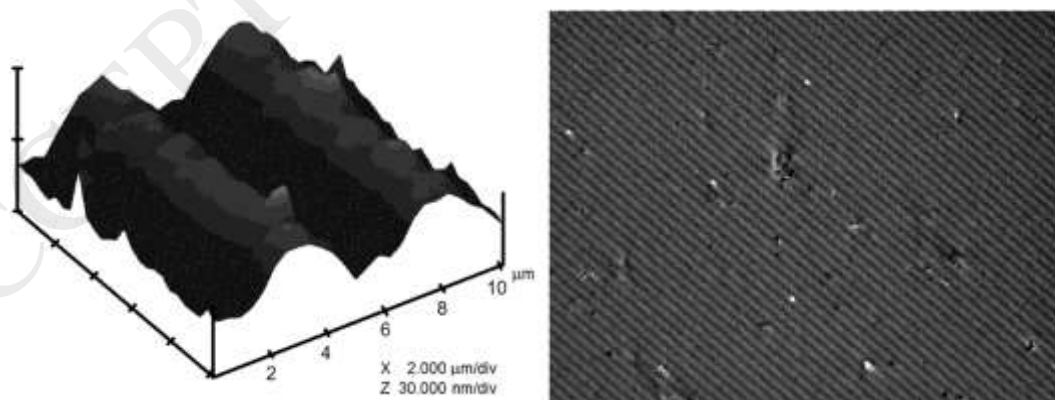


Figure 14. AFM (*left*) and POM (*right*) images of a SRG photo-inscribed in a film of the copolymer-IPFB complex **8**.

4. CONCLUSION

A polymer and a copolymer carrying lateral pyridylazobenzene groups were first synthesized and characterized by FTIR and NMR spectroscopies. These two polymers were then complexed with iodopentafluorobenzene rings through halogen bond as confirmed by FTIR. The combination of DSC, POM and XRD results indicated that these polymers and their complexes self-organize into smectic type arrangements (SmA and CrystE) or into aggregates with no order in the z-coordinates. The halogen-bonded copolymer complex showed a quite good photo-response in both writing/erasure experiments and SRGs inscription despite the bulkiness of the chromophore units that may photo-isomerize and move (at domain and micro-scale levels) under constraints imposed by the polymer chain.

Few halogen-bonded complexes showing both liquid crystal and photo-induced properties have been reported up to now. Here we have tested polymers carrying long rigid-rod like pyridylazobenzene groups which by themselves are mesogens and photo-active groups. These highly anisotropic groups can be complexed with some other halogen bond donors to look not only for improved photo-responsive properties but also for potential applications in optical elements.

Acknowledgements

Financial support provided by CONACYT Mexico under the project 242232 and the grants 420121 (C.V. Castro-Pérez, MSc thesis) and 385959 (N. Trejo-Carbajal, Posdoc) are gratefully appreciated. The technical assistance provided by Guadalupe Méndez (DSC), Julieta Sánchez ((FT-IR), Manuel Mata (XRD), and Antelmo Ruiz (Lab. facilities) is also appreciated.

ACCEPTED MANUSCRIPT

References

1. Z. Sekkat, W. Knoll, *Photoreactive Organic Thin Films*, Academic Press, San Diego 2002.
2. A. Emoto, E. Uchida, T. Fukuda, *Polymers* 4 (2012) 150.
3. H. Yu, T. Ikeda, *Adv. Mater.* 23 (2011) 2149.
4. A.A. Beharry, O. Sadvoski, G.A. Woolley, *J. Am. Chem. Soc.* 133 (2011) 19684.
5. A. Natansohn, P. Rochon, *Chem. Rev.* 102 (2002) 4139.
6. A.S. Matharu, S. Jeeva, P.S. Ramanujam, *Chem. Soc. Rev.* 36 (2007) 1868.
7. C. Cojocariu, P. Rochon, *Pure Appl. Chem.* 76 (2004) 1479.
8. A. Priimagi, M. Saccone, G. Cavallo, A. Shishido, T. Pilati, P. Metrangolo, G. Resnati, *Adv. Mater.* 24 (2012) OP345.
9. T. García, L. Larios-López, R.J. Rodríguez-González, G. Martínez-Ponce, C. Solano, D. Navarro-Rodríguez, *Polymer* 53 (2012) 2049.
10. A. Sobolewska, S. Bartkiewicz, A. Priimagi, *J. Phys. Chem. C* 118 (2014) 23279.
11. J. Vapaavuori, C.G. Bazuin, A. Priimagi, *J. Mater. Chem. C* 6 (2018) 2168.
12. M. Virkki, O. Tuominen, A. Forni, M. Saccone, P. Metrangolo, G. Resnati, M. Kauranen, A. Priimagi, *J. Mater. Chem. C* 3 (2015) 3003.
13. L. Cui, Y. Zhao, *Chem. Mater.* 16 (2004) 2076.
14. J.-M. Lehn, *Matter. Angew. Chem. Int. Ed.*, 52 (2013) 2836.
15. H. J. Sun, S. Zhang, V. Percec, *Chem. Soc. Rev.* 44 (2015) 3900.
16. T. Kato, N. Mizoshita, K. Kishimoto, *Angew. Chem. Int. Ed.* 45 (2006) 38.
17. G. Berger, J. Soubhye, F. Meyer, *Polymer Chem.* 6 (2015) 3559.

18. F. Fernández-Palacio, M. Poutanen, M. Saccone, A. Siiskonen, G. Terraneo, G. Resnati, O. Ikkala, P. Metrangolo, A. Priimagi, *Chem. Mater.* 28 (2016) 8314.
19. A. Priimagi, G. Cavallo, P. Metrangolo, G. Resnati, *Acc. Chem. Res.* 46 (2013) 2686.
20. M. Saccone, V. Dichiarante, A. Forni, A. Goulet-Hanssens, G. Cavallo, J. Vapaavuori, G. Terraneo, C.J. Barret, G. Resnati, P. Metrangolo, A. Priimagi, *J. Mater. Chem.* 3 (2015) 759.
21. J. Vapaavuori, I.T.S. Heikkinen, V. Dichiarante, G. Resnati, P. Metrangolo, R. G. Sabat, C.G. Bazuin, A. Priimagi, C. Pellerin, *Macromolecules* 48 (2015) 7535.
22. K.G. Gutiérrez-Cuevas, L. Larios-López, R. J. Rodríguez-González, B. Donnio, D. Navarro-Rodríguez, *Liq. Cryst.* 40 (2013) 534.
23. M.C. Tseng, O. Yaroshchuk, T. Bidna, A. K. Srivastava, V. Chigrinov, H.S. Kwok, *RSC Adv.* 6 (2016) 48181.
24. K. Okano, O. Tsutsumi, A. Shishido, T. Ikeda, *J. Am. Chem. Soc.* 128 (2006) 15368.
25. C. Ruslim, K. Ichimura, *Macromolecules* 32 (1999) 4254.
26. L. Larios-López, D. Navarro-Rodríguez, B. Donnio, D. Guillon. *Chem. Lett* 35 (2006) 652.
27. O.L. Torres-Rocha, L. Larios-López, R.J. Rodríguez-González, I. Felix-Serrano, D. Navarro-Rodríguez, *J. Molec. Liq.* 225 (2017) 251.
28. V. Kumar, D.J. Mulder, G. Cavallo, T. Pilati, G. Terraneo, G. Resnati, A.P.H.J. Schenning, P. Metrangolo, *J. Fluorine Chem.* 198 (2017) 54.
29. M.H. Palmer, M. Biczysko, K.A. Peterson, C.S. Stapleton, S.P. Wells, *J. Phys. Chem. A* 121 (2017) 7917.

30. B. Hawthorne, H. Fan-Hagenstein, E. Wood, J. Smith, T. Hanks, *Int. J. Spect.* (2013) 216518.
31. Q.J. Shen, H.Q. Wei, W.S. Zou, H.L. Sun, W.J. Jin, *CrystEngComm.* 14 (2012) 1010.
32. M. Rogojevov, B. Jordanov, L. Antonov, K. Hinrichs, *J. Mol. Struct.* 875 (2008) 540.
33. T. García, L. Larios-López, R.J. Rodríguez-González, J.R. Torres-Lubián, D. Navarro-Rodríguez, *ChemPhysChem* 13 (2012) 3937.
34. R. Duran, D. Guillon, P. Gramain, A. Skoulios, *J. Phys. France* 49 (1988) 1455.
35. D. Navarro-Rodríguez, Y. Frère, P. Gramain, D. Guillon, A. Skoulios, *Liq. Cryst* 9 (1991) 321.
36. Y. Ze-Fan, W. Jie-Yu, P. Jian, *Cryst. Growth Des.* 18 (2018) 7.
37. P. Huber, D. Wallacher, J. Albers, K. Knorr, *Europhys Lett.* 65 (2004) 351.
38. O.L. Torres-Rocha, R.J. Rodríguez-González, L. Larios-López, G. Martínez, C. Solano, D. Navarro-Rodríguez, *Polym. Int.* 63 (2014) 652.
39. J. Deng, W. Yuan, Z. Jia, G. Liu, *J. Phys. Chem. B* 118 (2014) 14536.
40. H. Menzel, B. Weichart, A. Schmidt, S. Paul, W. Knoll, J. Stumpe, T. Fisher, *Langmuir* 10 (1994) 1926.
41. S. Freiberg, F. Lagugné-Labarhet, P. Rochon, A. Natansohn, *Can. J. Chem.* 82 (2004) 1.
42. R.J. Rodríguez-González, L. Larios-López, D. Navarro-Rodríguez, *Liq. Cryst.* 38 (2011) 831.

43. C. de Santiago-Solís, R.J. Rodríguez-González, L Larios-López, O.L. Torres-Rocha, I. Felix-Serrano, G. Martínez-Ponce, D. Navarro-Rodríguez, J. App. Polym. Sci. (2017) 44819.
44. A. Natansohn, J.P. Rochon, J. Gosselin, S. Xiel, Macromolecules 25 (1992) 2268.
45. Y. Zhao, Pure Appl. Chem., 76 (2004) 1499.

ACCEPTED MANUSCRIPT